Vol. 20 (2026): Proceedings of 2026 International Conference on Materials Science, Energy Engineering and Automation Control (ICMSEAC 2026)
E-ISSN: 3105-0522 P-ISSN: 3105-0514
DOI: https://doi.org/10.70267/mseac.2026107115

The Impact of Clearance in the Front-wheel Steering Mechanism on Response Delay and Trajectory Deviation

Mingzhen Lv*

Department of Mechani, China University of Mining and Technology (Beijing), Beijing, China

**Corresponding author: Mingzhen Lv.*

Abstract

Single Pilot Operation (SPO) imposes stringent safety requirements on aircraft ground taxiing. However, the quantitative impact of mechanical clearance in the nose-wheel steering mechanism on response delay, trajectory deviation, and pilot workload remains insufficiently explored. In this study, a multi-body kinematic model with varying clearances was established using ADAMS to investigate this mechanism. By integrating a bicycle kinematic model, the strut steering angles were translated into aircraft taxiing trajectories under both open-loop and closed-loop (proportional control) conditions. The results demonstrate a non-linear positive correlation between clearance size and response delay. Crucially, automatic control exhibits an inherent compensation boundary, failing to eliminate the initial lag caused by the mechanical dead zone. Trajectory deviations, including lateral offset and heading angle errors, expand significantly with larger clearances and are further amplified at higher taxiing speeds. Workload assessments indicate that the 0.5 mm clearance (defined maintenance threshold in this paper) already induces a high monitoring workload for single pilots. Consequently, this paper recommends stricter maintenance thresholds, feedforward compensation strategies, and predictive heading indicators to ensure taxiing safety and alleviate pilot workload in SPO mode.

Keywords

front-wheel steering mechanism, response delay, single-pilot operation, workload, ADAMS simulation

1. Introduction

Since the 1950s, the aviation industry has steadily reduced crew sizes, gradually transitioning from five-person to two-person crews. As technologies have matured, the single-pilot operation mode has emerged as an important area for future exploration [1]. NASA research clearly indicates that pilot workload under abnormal operating conditions is the primary bottleneck limiting the feasibility of SPO [2].

According to statistics, more than 50% of aviation accidents occur during takeoff and landing. As the core component for controlling the direction of ground taxiing, the front-wheel steering mechanism's response characteristics directly affect the pilot's workload. However, the current studies have several major limitations [3-5]: they fail to account for the boundary conditions inherent to the mechanism's automatic clearance compensation. Most research results are presented in terms of trajectory deviation, without addressing workload assessment in SPO mode.

This paper focuses on the independent impact of mechanical clearance on response delay. Combined with a bicycle gliding model, it establishes for the first time a mapping chain linking “clearance—delay—trajectory deviation—operational load,” providing quantitative research findings under the SPO mode.

2. Modeling Principles and Simulation Scheme Design

2.1 Operating Principle of the Front-Wheel Steering Control System

The nose-wheel steering control system consists of three main components: the control unit, the actuation unit, and the feedback unit. Its operating principle is illustrated in Figure 1. In this paper, the PID algorithm is simplified to proportional control. The proportional gain *KP* is the proportional coefficient.

Figure 1: Nose Wheel Steering Control System Working Principle

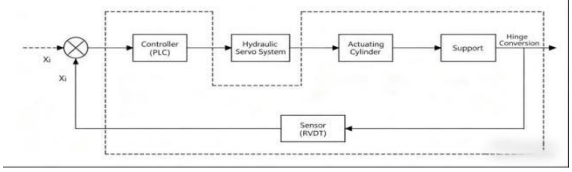

The research object of this paper focuses on the portion enclosed by the dashed box. It examines the delay effect of clearance on motion transmission separately.

2.2 Kinematic Modeling of the Dual-Actuator Front-Wheel Steering Mechanism

2.2.1 Mechanism Configuration and Geometric Equations

In the aviation standard, the motion states of the front-wheel steering mechanism within a turning cycle are extracted into three nodal states. As shown in Figure 2.

Figure 2: Three States of Nose Wheel Steering Mechanism [3]

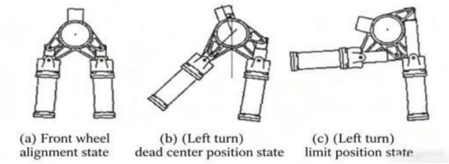

Based on the state definition, this paper establishes a topological model of the front-wheel steering mechanism. It simplifies it to a four-bar linkage composed of rigid bodies, including struts, rocker arms, left- and right-hand actuators, and piston rods. Geometric parameters are defined: strut radius R, rocker arm length r, joint distance L, initial angle α, the piston rod displacement s, and strut rotation angle δ. Satisfy the closed-loop constraint:

$$L^2 + [2(R+r)\sin\left(\frac{\theta}{2}\right)]^2 - (L+s)^2 - 2L\left[2(R+r)\sin\left(\frac{\theta}{2}\right)\right]\cos\left(90^\circ + \frac{\theta}{2} + \alpha\right) = 0 \tag{1}$$

2.2.2 Establishment of the Driving Equation

Nie Qing [3] used the displacement of the piston rod as the input signal fed to the controller and found that, by employing a hydraulic system with excellent tracking performance, the input signal could be closely matched to the output signal. Therefore, it is reasonable to neglect the intermediate processes involved in signal transmission. This paper applies a displacement drive to the right piston rod. The driving function is consistent with the literature. This simplification eliminates the interference of the hydraulic system’s dynamics on response delay, allowing the study to focus solely on the effect of the clearance itself on response transmission.

2.2.3 Simulation Condition Design

ADAMS (Automatic Dynamic Analysis of Mechanical Systems) has been widely applied in the field of aerospace mechanism dynamics research [6-8]. This paper uses ADAMS to simulate and build a model of the front-wheel steering mechanism that includes clearances. Clearance is introduced at the piston rod-strut interface.

To simulate the entire service life of the mechanism, from new to severely worn conditions [9], this paper sets forth five wear scenarios. For each wear scenario, both open-loop and closed-loop control strategies are designed. The scenarios are shown in the table below.

Table 1: Simulation Case Settings

Case	Amount of clearance(mm)	Control mode	Description
1	0	Open-loop	Ideal benchmark
2	0.1	Open-loop	Slight wear
3	0.3	Open-loop	Medium wear
4	0.3	Closed-loop	Medium wear
5	0.5	Open-loop	Maintenance threshold
6	0.5	Closed-loop	Maintenance threshold
7	1.0	Open-loop	Heavy wear
8	1.0	Closed-loop	Heavy wear

2.3 Definition and Extraction of Response Latency

In this paper, response delay is defined as the duration by which the actual strut rotation curve lags behind the onset time of the ideal model's response. In an ideal mechanism, the time difference between the signal input and the strut rotation is determined solely by the system's inertia and typically amounts to less than 20 milliseconds. However, in mechanisms with clearances, the additional delay arises from the dead-zone effect induced by the clearance. By comparing actual behavior with the ideal model, this paper can eliminate the influence of system inertia.

Let the response initiation time for the ideal model be t_{ideal}, and the response initiation time for the gap model be t_{act}, The response delay is defined as:

$$\Delta t = t_{act} - t_{ideal} \quad (2)$$

A small numerical value exists in the steering column angle during the free-travel phase. Therefore, this paper selects a threshold angle of 0.0001°—a value slightly greater than the level of numerical noise—which effectively filters out spurious fluctuations while remaining far smaller than the actual response angle, thereby accurately capturing the physical moment when the front wheels begin to respond.

2.4 Aircraft Taxiing Kinematic Model

To transform the strut turning curve into a sliding trajectory, this paper adopts the bicycle model, as shown in the Figure 3. It is assumed that the aircraft slides at a constant speed *v*, and inertial forces are neglected, making this model suitable for low-speed sliding conditions [10].

Figure 3: Bicycle Model Principle

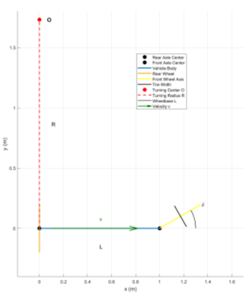

The kinematic equations for the aircraft's low-speed ground taxiing are as follows:

$$\Psi' = \frac{v}{R} = \frac{v\tan(\delta)}{L} \quad (3)$$

$$x' = v\cos\psi \quad (4)$$

$$y' = v\sin\psi \quad (5)$$

Ψ represents the heading angle during the turn, with the X-direction defined as 0; v is the turning speed; R is the turning radius; L is the fuselage length, which, referencing the A320 in this paper, is set at 12.64 m; δ is the difference between the desired heading angle and the actual heading angle.

The heading angle is influenced by the turning speed and the strut's turning angle. The relationship between heading angle and time is:

$$\Psi(t) = \int_0^t \frac{v}{L} \tan(\theta(t) - \Psi(t))dt \quad (6)$$

At the same speed, the larger the steering angle of the support strut, the greater the cumulative heading angle accumulated over the same period, and the faster the rate of change of the heading angle. Under the same operating conditions, the higher the gliding speed, the stronger the front wheel's ability to track the heading angle.

The heading angle difference is related to the turning speed and the difference in support strut angles. The equation is:

$$\Delta\Psi' = \frac{v}{L}\{\tan[\theta(t) - \Psi] - \tan[\theta(t)_{ideal} - \Psi_{ideal}]\} \quad (7)$$

$$\Delta\Psi' = \frac{v}{L}[\tan(\delta) - \tan(\delta_{ideal})] \quad (8)$$

Since the sliding occurs under the same mechanism, δ are approximately equal. Obtain the linear deviation equation:

$$\Delta\Psi' + vk\Delta\Psi = vk\Delta\theta(t) \quad (9)$$

The term $vk\Delta\Psi$ can be regarded as a damping term. When the damping coefficient vk is relatively small, the heading angle deviation can be approximated as being proportional to the velocity and angle difference.

The trajectory depends on the speed and the variation of the heading angle during turns:

$$x(t) = v\int_0^t \cos(\Psi(t))dt \quad (10)$$

$$y(t) = v\int_0^t \sin(\Psi(t))dt \quad (11)$$

At the same speed, the larger the support strut's turning angle, the greater the accumulated heading angle and the sharper the turning trajectory. Under the same operating conditions, while speed acts as a multiplicative factor that amplifies the trajectory, it also affects the tracking of the heading angle; thus, the higher the speed, the more pronounced the trajectory's curvature.

2.5 Load Assessment Method

Throughout the aircraft's entire turn maneuver, the ideal trajectory serves as the reference centerline. In dual-pilot mode, the co-pilot is responsible for monitoring the lateral deviation from the trajectory and the heading-angle deviation. The pilot-in-command only needs to actively make corrections. However, in SPO mode, all tasks are performed solely by the pilot. Under adverse operating conditions, this significantly increases the pilot's workload.

This paper uses a lateral offset of 0.5 meters as the trigger condition for manual correction. The value is adopted as a simulation assumption based on engineering rationality (approx. 1/15 of A320 main gear track width and well below taxiway width), providing a conservative correction trigger without excessive pilot intervention. When manual correction is not triggered, only the heading angle deviation needs to be monitored. To reasonably define the heading angle deviation that requires monitoring, this paper draws on research in human factors engineering on the "heading discrimination threshold" [11], defining this metric as the minimum heading angle deviation at which the correct detection rate reaches 84%. Typically, this value is set at 1°.

Taking the driver workload in the two-person mode as the reference and normalizing it, and given that current publicly available literature has not yet provided precise decomposition coefficients for the manipulation-monitoring workload in SPO mode, this paper, based on the statistical rule from NASA TLX [12], assumes a monitoring workload weighting coefficient α= 0.5 and establishes the relative monitoring workload:

$$\eta = 1.0 + \frac{\alpha t}{a} \quad (12)$$

Based on references [13], *a* is set at 4 seconds. ηmust not exceed 1.5; otherwise, it will be considered dangerous.

3. Verification and Analysis of System Simulation Result

3.1 Simulation Results and Delay Characteristic Analysis

3.1.1 Simulation Results and Validation

The geometric parameters are not publicly available. Estimated based on AMM specifications [14]:

R=75mm, r =101.2mm, L =135mm, α =0.5625. All subsequent experimental studies will be based on these parameters.

As verification, the curve derived from the geometric equations closely matches the simulation curve, with a maximum error of only 0.0003°, which is negligible. This confirms the rationality of the simulation experiment design.

To verify the reasonableness of the feedback control, set *KP* = 0. The experiment showed that when the communication step size was 0.0012 s, the difference in support strut angles between the open-loop and closed-loop conditions was identical.

Since the proportional control introduced in this paper is not intended to precisely simulate the actual control law of an aircraft BSCU, but rather serves as a feedback mechanism to reveal the physical limitations inherent in control compensation. Therefore, this paper set *KP* = 0.6 and concluded that no further gain optimization is necessary.

3.1.2 Delay Characteristic Analysis

Simulation experiments were conducted for each operating condition. Angle difference increase with clearance and the response delay results were shown in Table 2.

Table 2: Response Delay Time Under Different Conditions

Case	Response delay time(s)
2	0.0526
3	0.1041
4	0.0884
5	0.1380
6	0.1173
7	0.2002
8	0.1712

In the Figure 4(a), exhibits a monotonically increasing trend with a gradually decreasing slope. In the initial response phase of the piston rod—where acceleration starts from zero and eventually reaches a steady-state value—the slope of the clearance-delay relationship progressively diminishes. In the figure 4(b), within the maintenance threshold range, the compensation efficiency drops significantly. This indicates that the time during which the piston rod transmits motion freely within the clearance cannot be eliminated by feedback control.

Figure 4: Clearance-Delay Fitting Curve and Clearance-Compensation Effect Fitting Curve

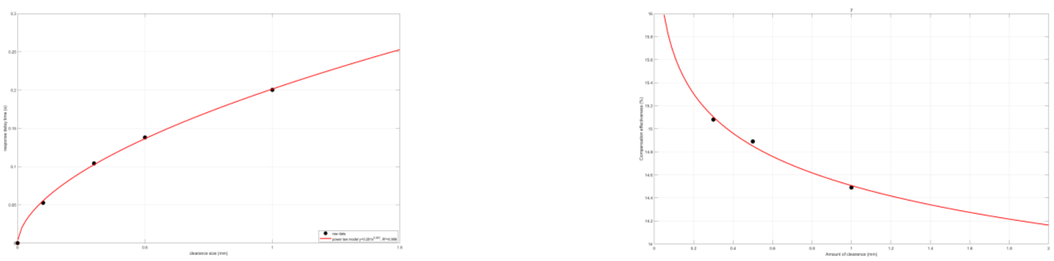

(a) (b)

3.2 Analysis of Slippage Trajectory Deviation

3.2.1 Trajectory Offset Calculation Based on Gap Influence

To comprehensively assess the aircraft trajectory deviations under the influence of delay, three types of deviations are defined: heading-angle deviation, turning-point deviation and maximum lateral deviation.

Throughout the entire turning process, the track angles under all conditions first fall below the ideal state and then rise above it. The times at which the heading angle differences reach their extreme values coincide with the times when the turning angle differences switch from positive to negative; the heading angle deviation increases with clearance. Thus validating the inference made in Section 2.4. As can be inferred from the heading-angle-difference versus time curve, the trajectory under clearance conditions initially lies to the right of the ideal-trajectory curve. Subsequently, the trajectory's slope rapidly increases, crosses the ideal trajectory, and then gradually deviates to the left. The greater the clearance, the larger the deviation. This is consistent with the Figure 6 shown.

Figure 6: Heading Angle Difference-Time Curve and Final Trajectory Comparison

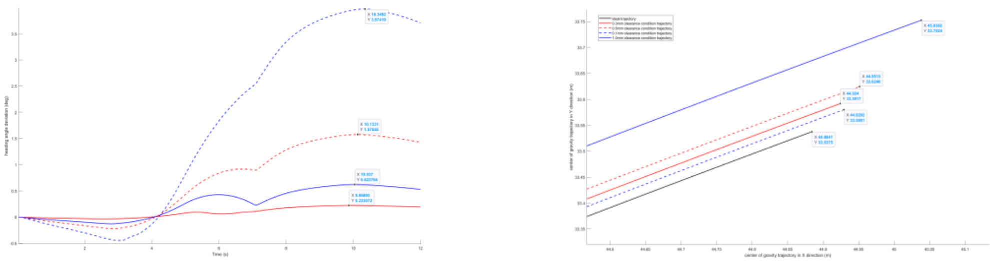

V represents the maximum permissible airspeed during aircraft turns, which is 5 m/s.[15]From the geometric relationship, turning-point deviation is:

$$s = v \times \Delta t$$

Using 0.0005 m Y-displacement as reference, X-displacements were observed to study trajectory deviation after the inflection point to investigate the subsequent trajectory deviation.

To quantitatively reflect the degree of trajectory deviation during turning, this paper calculates the shortest perpendicular distance between the actual and ideal trajectories at each moment, with particular emphasis on the maximum lateral deviation. As shown in Table 3.

Table 3: Deviations

Case	Inflection point offset(m)	X-Direction offset(m)	Maximum lateral offset(m)
2	0.2630	0.066	0.0183
3	0.5205	0.174	0.0304
4	0.4420	0.126	0.0108
5	0.6900	0.270	0.0475
6	0.5865	0.240	0.0231
7	1.0010	0.458	0.1222
8	0.8560	0.318	0.0619

Tiny response delay can become dangerous when amplified by movement, but the small Y-direction offset at the inflection point prevents immediate danger. After the strut's corner response, the piston rod accumulates energy and impacts the strut, rapidly increasing the corner rate under clearance — effectively compensating for the displacement caused by the delay. Small clearances enable high-frequency oscillations, making this self-compensation particularly effective. Proportional control reduces offset, but larger gaps worsen compensation performance. This reveals that once a response has begun, control compensation has inherent limitations. Sensitivity Analysis of Velocity.

3.2.2 Sensitivity Analysis of Velocity

Add two high-speed turning scenarios at 10 m/s and 15 m/s.

Compare ideal center-of-gravity trajectories at different turning speeds, it can be seen that the greater the speed, the larger the trajectory shape, the more pronounced the curvature. At a turning taxiing speed of 15 m/s, the heading angle has already nearly returned to its original value. Experiments also found that the heading-angle deviation value exhibits an approximately linear relationship with the turning speed. In the context of this paper, vk can be regarded as a small damping coefficient, thereby validating the inference presented in Section 2.4.

To analyze the impact of turning speed on turning safety, extract the above-mentioned offset.

Table 4: Deviations at Different Speeds

Case	Inflection point offset(m)		X-Direction offset(m)		Maximum Lateral Offset(m)	
	Velocity(m/s)		Velocity(m/s)		Velocity(m/s)	
	10	15	10	15	10	15
2	0.526	0.7890	0.168	0.270	0.0546	0.0932
3	1.041	1.5615	0.422	0.702	0.0706	0.1090
4	0.884	1.3260	0.312	0.504	0.0274	0.0452
5	1.380	2.0700	0.647	1.062	0.1100	0.1689
6	1.173	1.7595	0.504	0.837	0.0476	0.0780
7	2.002	3.0030	1.127	1.854	0.2907	0.4496
8	1.712	2.5680	0.828	1.386	0.1262	0.1872

Higher speeds reduce the mechanism's ability to compensate for turning point offset. After angular response, greater gliding speed shortens the time needed for the center of mass to reach 0.005 m in the Y-direction. However, compensation relies on the piston rod's impact-and-vibration process within the clearance—too slow to complete an adjustment cycle in a short period. Data show that higher turning speed increases both the maximum lateral offset and its rate of growth. Consequently, trajectory deviation caused by delay is amplified at high speeds.

3.3 Calculation of Operational Load under Single-Pilot Operation Mode

According to the data presented in Section 3.2, under a turning speed of 5 m/s, the trajectory deviations remain within the correction range. However, in the case with the largest gap, the heading angle deviation has remained above the monitoring threshold for an extended period. Therefore, in this study, the primary source of workload is the pilot's continuous monitoring of the heading angle deviation. The workload for each operating condition is shown in Table 5.

Table 5: Workload Assessment Under Various Conditions

Case	Monitoring duration(s)	Workload value
2	0	1
3	0	1
4	0	1
5	4.68	1.585
6	3.97	1.496
7	6.84	1.855
8	6.67	1.834

Under the current maintenance threshold in SPO mode, with a closed-loop operating condition at KP=0.6, high monitoring workload has already been triggered, necessitating the formulation of new engineering recommendations.

3.4 Compensation Strategies and Engineering Recommendations

3.4.1 Compensation Boundary for Automatic Control

Experimental data show that control compensation cannot eliminate response delay, and the larger the clearance, the poorer the compensation effect becomes. While self-regulation of the mechanism and closed-loop control can compensate for the shift in response delay, they cannot eliminate trajectory deviation. As clearance increases, the magnitude of trajectory deviation grows rapidly. These results demonstrate that there are inherent limits to automatic control.

The above results can be explained by the underlying physical mechanisms: Under closed-loop operating conditions, the front-wheel steering mechanism still follows the “idle stroke—collision” mechanism. The collision between the piston rod and the strut necessarily involves an idle stroke. After the collision response, since the piston rod exerts an impact force on the strut, the strut cannot move along with the piston rod. Compensation can only be achieved by reducing the interval between successive collisions, thereby minimizing the deviation.

3.4.2 Engineering Recommendations for Single-Pilot Operation Mode

Based on the scenario described in this paper, the following engineering recommendations are proposed for the single-pilot flight mode: At the mechanical design level, given that the maintenance threshold load exceeds the specified limit, it is recommended to set the maintenance thresgold to less than 0.5mm. At the control strategy level, to overcome the inherent limitations of automatic control compensation, it is recommended to introduce a feedforward compensation strategy to send control signals in advance, thereby offsetting the initial lag. At the human-machine interaction level, given the high workload from continuous monitoring, it is recommended to add a predictive heading indicator to reduce the monitoring burden. These improvements can fully leverage the control compensation capability, ensuring both safe taxiing and a balanced workload in SPO mode.

4. Conclusion

The main conclusions of this article are as follows:

Automatic control compensation has inherent limitations; the larger the gap, the greater the trajectory deviation. Moreover, high-speed gliding can exacerbate the risk of deviation caused by the gap. Under SPO mode, the current maintenance threshold has already led to a high monitoring workload, and it is recommended to propose new engineering requirements.

This paper focuses on the institutional response itself and does not account for practical factors such as hydraulic system dynamics, tire slip angles, and runway friction. It also does not specify exact boundary values. In future studies, joint optimization across multiple parameters and research on the effects of clearance in all-electric steering mechanisms could be conducted.

References

[1] Wang M. Single Pilot Operation Mode Technology[J]. Acta Aeronautica et Astronautica Sinica, 2020.

[2] Comerford, Doreen, et al. “NASA's single-pilot operations technical interchange meeting: proceedings and findings.” Technical Interchange Meeting. No. ARC-E-DAA-TN8313. 2013.

[3] Nie Q, Nie H, Zhang M. Design and Simulation Analysis of Dual-Actuator Nose Wheel Steering System for Large Civil Aircraft[J]. Journal of Nanjing University of Aeronautics and Astronautics, 2012, 44(4).

[4] Zhang, Ming, Rongmin Jiang, and Hong Nie. “Design and test of dual actuator nose wheel steering system for large civil aircraft.” International Journal of Aerospace Engineering 2016.1 (2016): 1626015.

[5] Zhou, J. (2020). Research into Nose Wheel Steering Deviation Angle Calculation of a Civil Aircraft. Journal of Physics: Conference Series.

[6] Deja, J., Dayyani, I., Nair, V., & Skote, M. (2023). More Electric Aircraft Conversion to All-Electric During Ground Operations: Battery-Powered Landing Gear Drive System. IEEE Transactions on Transportation Electrification, 10(1).

[7] Hui W X, Jia J Q, Zhao C, Gao C, Wang M, Liu Y Y. Analysis of the Influence of Aircraft Tractor Braking Operation on Nose Landing Gear[J]. Science Technology and Engineering, 2024(21).

[8] Jin G G, He S, Wei Z, et al. Dynamic Analysis of Planar Flexible Six-Bar Mechanism with Multiple Joint Clearances[J]. Journal of Tiangong University, 2024, 43(4).

[9] AIRBUS. A320 Aircraft Maintenance Manual (AMM), Task 32-22-13: Adjustment of the NLG Aft Door Gaps[R]. Toulouse: Airbus, 2011.

[10] Sathish, S., Suryanarayanan, L., Vyas, J. J., & Balamurugan, G. (2020). Applicability of Tricycle Modelling in the Simulation of Aircraft Steering System. In Springer Proceedings. Springer, Singapore: 171-183

[11] Sharples, S., & Shorrock, S. (2014). Contemporary Ergonomics and Human Factors 2014: Proceedings of the international conference on Ergonomics & Human Factors 2014, Southampton, UK, 7-10 April 2014.

[12] Hart, Sandra G., and Lowell E. Staveland. “Development of NASA-TLX (Task Load Index): Results of empirical and theoretical research.” Advances in psychology. Vol. 52. North-holland, 1988. 139-183.

[13] Li, Chongfeng, Ruishan Sun, and Xing Pan. “Takeoff runway overrun risk assessment in aviation safety based on human pilot behavioral characteristics from real flight data.” Safety science 158 (2023): 105992.

[14] Airbus. Aircraft Maintenance Manual (AMM): A320[M]. Toulouse: Airbus, 2024.

[15] Airbus. A320/A321 Flight Crew Training Manual (FCTM)[S]. Airbus, 2021.

Funding

This research received no external funding.

Conflicts of Interest

The authors declare no conflict of interest.

Acknowledgment

This paper is an output of the science project.